

CoMoGen: COntrrollable MOtion Dynamics and Interactions with Mask-Guided Video GENERation

Adil Meric¹, Lin Geng Foo², Mert Kiray^{1,3,4}, Benjamin Busam^{1,3,4},
Rishabh Dabral², and Christian Theobalt²

¹ Technical University of Munich

² Max Planck Institute for Informatics, Saarland Informatics Campus

³ Munich Center for Machine Learning (MCML)

⁴ Obsphera

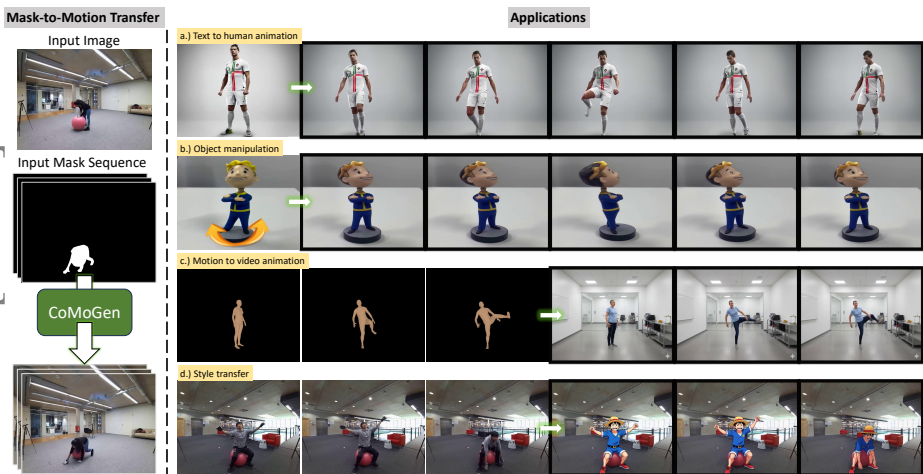


Fig. 1: Overview. Given a single input image and a binary mask sequence (left), CoMoGen generates videos where the masked subject follows the steering mask sequence while the model generates plausible interactions with the surroundings. On the right, we show applications: a) Text to human animation from textual motion and rendered masks, b) Object manipulation conditioned on a mask sequence, c) Motion to video animation from generated motion and first frame, and d) Style transfer, animating translated images while preserving motion.

Abstract. We present CoMoGen, a controllable video generation framework that generates realistic interactive dynamics from a single binary mask sequence conditioned on an input image. CoMoGen introduces a lightweight MaskAdapter that encodes binary mask sequences into a latent residual signal, injected into the Multi Modal Diffusion Transformer (MMDiT) model through a cosine-weighted schedule. Unlike the hierarchical coarse-to-fine design of UNet architectures, MMDiT operates as a sequence of uniform transformer blocks, making it difficult to identify which layers are responsible for the motion generation. Therefore, we propose a novel way to determine “Motion Layers” operating in the attention

space of MMDiT. We fine-tune the model by using Low-Rank Adaptation (LoRA) to the Motion Layers, without requiring any architecture change in the MMDiT. This selective adaptation enables our method to focus on motion-critical components, yielding reduced computational cost. Despite its simplicity, CoMoGen enables precise subject motion and plausible interactions with surrounding humans, objects, and scenes. Comprehensive experiments on different datasets show that CoMoGen consistently outperforms prior controllable video generation methods and achieves state-of-the-art performance in motion fidelity and perceptual realism. Project page: mericadil.github.io/CoMoGen.

Keywords: Video Generation · Generative Models · Conditional Generation

1 Introduction

Recent advances in video generation [7, 8, 22, 24, 27, 51, 55] have made it possible to generate visually appealing and temporally consistent videos from given text or image inputs. Although these models often exhibit high-quality appearance, making them controllable has emerged as the next frontier for research. In particular, controlling how objects move and interact remains a central challenge. Realistic motion requires an ability to reason about physical relationships between scene entities (humans, objects, and their surroundings) and model sparse video guidance into coherent spatiotemporal dynamics. Without this ability, the generated motion may be temporally smooth yet physically implausible, failing to capture contact, collision, or consequential motion in the environment.

Existing controllable video generation frameworks [1, 9, 16, 28, 30, 32, 38, 39, 43, 47, 53, 54, 56, 61] are mostly built on explicit dense signals such as optical flow or trajectories. These control signals offer structured guidance but often require extensive pre-processing [42], domain-specific annotations [30, 62], or additional noise-warping machinery [9]. Some recent works employ ControlNet [59] to introduce such control signals [1, 4, 16, 19, 30]. However, ControlNet typically relies on a trainable copy of the backbone with added zero-initialized layers and produces control residuals across the network, substantially increasing parameter count and training/inference cost, and making controllability dependent on learning how much to inject at each layer.

In this work, we introduce CoMoGen, a framework that generates videos with controllable motion while exhibiting interactive dynamics from the mask guidance. As shown in Fig. 1 (Mask-to-Motion Transfer), CoMoGen takes a single input image and a binary mask sequence that specifies where the controlled subject should appear in each frame, and generates a coherent video that follows this motion while having coherent interactions with the scene. In other words, beyond following the given mask, the model also produces plausible interactions consistent with the context. We further show several applications (see Fig. 1, Applications): (a) Text-to-human animation, where human body is reconstructed from single image [17] and a motion diffusion model (MDM) [50] gen-

erates a mask sequence that drives CoMoGen; (b) Object manipulation, where hand-driven object motion is captured in a short video, masks are extracted (Grounding DINO [33] + SAM2 [44]), and CoMoGen animates the input image accordingly; (c) Motion to video animation, where an MDM-generated mesh sequence is converted to a realistic first frame via image-to-image transfer [18] and then animated using the mesh masks; and (d) Style transfer, where we apply image-to-image stylization [18, 29] to the input image and generate a stylized video guided by the same masks.

To realize this, we propose a lightweight MaskAdapter that converts a spatiotemporal mask sequence into a latent residual direction. The adapter produces a directional update to the latent variables that biases the generative velocity field toward motions of the moving mask. The MaskAdapter is implemented with two convolutional layers followed by a linear projection, and leaves the base model unchanged. The predicted latent residual direction can be injected into DiT blocks (together with a little LoRA fine-tuning) for mask-guided video generation.

Importantly, to keep our method as lightweight and efficient as possible, we aim to minimize the number of added parameters. Yet, this is not straightforward; in contrast to the hierarchical coarse-to-fine nature of earlier UNet architectures [7, 8] for diffusion-based video generation, modern Multi Modal Diffusion Transformers (MMDiT) [14] perform combined spatial and temporal reasoning throughout a sequence of MMDiT blocks, making it unclear where motion is primarily formed. Inspired by insights from DiTCTRL [10], StableFlow [3], and TAVID [26] we analyze Video-to-Text and Text-to-Video attention alignment between subject tokens and mask regions across inference steps. By measuring the alignment between mask regions and attention maps, we identify a sparse subset of DiT blocks and denote them as Motion Layers, which contribute most to dynamic behavior. We then inject the mask conditioning primarily through these Motion Layers and apply selective Low-Rank Adaptation (LoRA) [25] only on them, concentrating learning capacity where motion is formed while keeping the remaining blocks frozen. This results in a lower parameter and lower cost control mechanism compared to ControlNet-style designs [1, 16, 19, 30] that learn per-layer residual injections across the full network.

Considering that early iterative steps determine global structure and motion while later steps refine details [11, 13, 21, 37], we further introduce a cosine-decayed residual schedule: it weights the mask guided latent shift strongly at early steps and smoothly fades it to zero toward the end. This matches our empirical observation that motion-relevant alignment signals peak in earlier steps and diminish as refinement progresses.

CoMoGen provides a unified solution for motion control across diverse settings, including human-to-object and object-to-object interactions. The approach is efficient and generalizes across varying spatial resolutions, sequence lengths, and out-of-distribution visual domains. Quantitative and qualitative results on BEHAVE [6] and CLEVRER [57] demonstrate that CoMoGen outperforms prior controllable video generation methods [1, 9, 30] and establishes state-of-the-art

performance in motion fidelity and generation quality. Training CoMoGen only on videos from the BEHAVE dataset, we demonstrate this capability through diverse applications in Fig. 1, transferring the same mask-to-motion principle to real-world scenes, enabling object manipulation, and supporting style transfer while preserving motion control. Please see the Appendix for the applications’ setups and details.

Our main contributions are as follows:

- We introduce CoMoGen, a mask-driven controllable video generation framework that enables interactive dynamics from a given input image and a binary mask sequence.
- We propose a lightweight MaskAdapter with cosine-weighted latent modulation that enables controllable motion without architectural changes to the base model.
- We identify and leverage a subset of transformer blocks, denoted as Motion Layers, that are most responsible for motion generation in MMDiT. By injecting conditioning and applying LoRA only on these layers, we reduce computational overhead compared to ControlNet-style full network residual injection while preserving generation quality.

2 Related Work

Video Generation with Diffusion Models. Diffusion models have become a dominant paradigm for video synthesis due to their scalability and sample quality. Early works adapted image-based UNets to the video domain [22,24], but suffered from frame drift and limited sequence length. Subsequent approaches introduced temporal attention, latent-space modeling [7, 8, 20], and noise alignment [12] to improve temporal consistency; yet UNet approaches often scale poorly due to limited temporal modeling and high spatiotemporal cost. To overcome this, recent advances leverage diffusion transformers (DiT) [27, 51, 55, 63], enabling longer videos, higher resolutions, and better motions. Latest models match the power of DiT with flow-matching and generate impressive results [27, 51]. However, these generative video models are typically conditioned only on text or images with limited control over the generated motion and interactions. Recently, DiTctrl [10] was proposed to address limitations of short video generation by performing MMDiT attention analysis to improve consistency in a tuning-free manner. TAVID [26] introduces a loss in attention space for target-to-mask alignment. Stableflow [3] determines vital layers, layers that are essential for image formation, by measuring the deviation in image content when bypassing each layer individually. Inspired by DiTctrl, TAVID, and StableFlow in the image domain, we analyze attention layers to locate Motion Layers, and then combine LoRA with a MaskAdapter to achieve efficient, lightweight controllability.

Controllable Video Generation via Explicit Signals. To address controllability, several methods incorporate external motion signals. Trajectory-based approaches encode object paths as sparse points, bounding boxes, or dense masks

and integrate them into video generation pipelines [15, 30, 62]. Control signals are fused through dedicated modules like trajectory encoders [62], ControlNet-style adapters [1, 30], or attention-guided layers [52, 58]. In particular, several works [1, 2] focus on mask-conditioned video generation via ControlNet adapters, yet ControlNet adapters contain large numbers of parameters which often require considerably large amounts of training data. Others explore flow-guided control by warping the noise in temporal dimension [9], enforcing temporal correlation while maintaining flexibility. FreeTraj [42] achieves trajectory control without tuning by adapting the sampling schedule. While effective, these approaches often rely on curated annotations or handcrafted motion formats. Moreover, the fine-tuning approaches often require a large amount of carefully curated data together with many trainable parameters, while the training-free methods face issues handling interactions of objects with the surroundings. Differently, we aim to perform mask-guided video generation with dynamics and interactions, in a manner that is efficient, architecture independent, and generalizable.

Interactive Dynamics and Physical Modeling. Modeling object interactions and physical causality poses additional challenges. InterDyn [1] introduces a binary mask sequence as a minimal control signal to drive physical interactions, enabling realistic modeling of physical events such as collisions and contact propagation by training a ControlNet style condition network. CosHand [49] takes a more limited approach focused on static hand-object transitions. However, these methods often require large amounts of curated data and add many additional parameters to their model for fine-tuning, which we eschew in our work. Recent work also explores video generation with the aid of physical simulators: MotionCraft [38] combines a physical simulator with an image generation model for video generation, and MotionCtrl [53] blends multiple motion controllers for better generalization while using training data from a physical simulator. Yet, these methods using physical simulation engines are often limited in capability, e.g., facing difficulty in modeling human motions, object deformations, etc. In contrast, CoMoGen captures interactive effects without depending on simulation engines, which has the advantage of simplicity and does not face limitations brought by the physical simulators.

3 Preliminaries

3.1 Diffusion Transformers (DiT) and Multi Modal DiT

Classical diffusion models [7, 23, 45, 46, 48] rely on UNet backbones with encoder-decoder structures and skip connections, and incorporate conditioning via cross-attention [7, 45, 46]. While effective for images, these designs often scale poorly to videos due to limited temporal modeling and high spatiotemporal cost.

Diffusion Transformers (DiT) [40] replace convolutional UNets with transformer blocks operating on latent tokens, offering global receptive fields and strong text-image alignment; however, the contribution of individual layers becomes less explicit. Building on this, Multi Modal Diffusion Transformers (MMDiT)

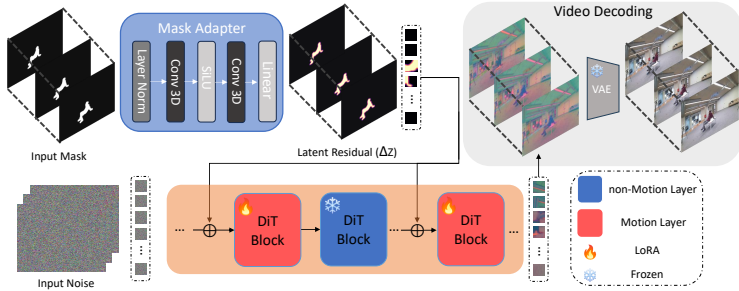


Fig. 2: Framework overview. Given a spatiotemporal binary mask sequence, we first downsample it to latent resolution and project it into a latent residual ΔZ using a lightweight MaskAdapter. During image-to-video generation, we inject this residual by modulating the current noised video latent at the transformer input, and propagate the conditioning through only the identified Motion Layers (DiT Blocks marked in red), while keeping the remaining blocks frozen (DiT Blocks marked in blue). LoRA modules are applied exclusively to the Motion Layers to adapt motion behavior efficiently without disturbing the backbone’s spatial priors. The strength of the injected residual is controlled by a reverse cosine schedule, enforcing strong mask guidance in early denoising steps, where coarse spatial structure and motion are formed, and gradually fading to zero toward the final steps to preserve visual quality.

[14, 27] jointly processes multimodal tokens (e.g., text and video latents) by combining self-attention and cross-attention. This formulation is adapted in many modern video generators [27, 51, 55].

3.2 Rectified Flow Matching

Rectified flow [14] is an iterative denoising technique, which learns a velocity field $v_\theta(x_t, t)$, often parameterized by a deep model θ . The velocity field maps a noisy latent $x_t = (1 - t)x_0 + t\epsilon$ toward clean data x_0 , where t is the time step and ϵ is random noise. Formally, the training loss is:

$$\mathcal{L}_{\text{FM}} = \mathbb{E}_{x_0, \epsilon, t} [\|v_\theta(x_t, t) - (x_0 - \epsilon)\|_2^2]. \quad (1)$$

Unlike diffusion, flow matching follows straight trajectories between data and noise, causing faster convergence and stable gradients which is used in state-of-the-art video generation models [27, 51].

4 Method

We address interactive dynamics between objects given a controllable mask signal. Given an input image $I \in \mathbb{R}^{H \times W \times 3}$ and a sequence of binary masks $M \in \mathbb{R}^{T \times H \times W}$, CoMoGen generates a video $V \in \mathbb{R}^{T \times H \times W \times 3}$, in which the target subject (a person) follow the motion defined by the provided mask sequence,

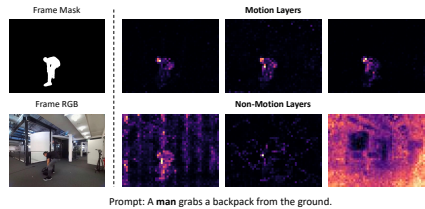
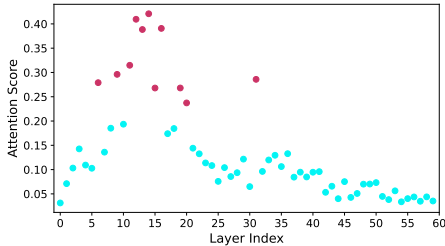


Fig. 3: Attention score over layers. Motion Layers (marked in red) show consistently higher subject-mask alignment than Non-Motion Layers (marked in blue).

Fig. 4: Attention visualization. Motion Layers concentrate attention on the masked subject token; non-motion layers show weak alignment.

resulting in coherent and physically plausible interactions with the surrounding environment.

To this end, we employ a MaskAdapter that maps the input binary masks to a latent residual (delta), representing the direction of change in the latent space (see Fig. 2). However, instead of learning the MaskAdapter residuals for all layers, we first identify the *vital* layers responsible for mask-video correlation, dubbed Motion Layers. Building on our analysis of Motion Layers, we apply LoRA [25] only to these transformer blocks enabling efficient fine-tuning focused on motion-critical components. This selective adaptation preserves the base model’s strong spatial priors while enhancing controllable motion generation. We further introduce a reverse cosine scheduler to modulate the strength of this delta across the steps of the flow matching process: its weight starts at 1 for the first step and gradually decays to 0 by the final step.

We first describe how we identify the Motion Layers important for video motion generation in Section 4.1. We then present the proposed MaskAdapter architecture in Section 4.2, including our layer-selective residual injection strategy and the corresponding LoRA training restricted to these Motion Layers. Finally, we detail our reverse cosine scheduler for cosine-weighted delta injection which is designed to preserve the base model’s fine detail capacity while enabling controllable motion in Section 4.3.

4.1 Identifying Motion Layers

Building on the MMDiT architecture, we first examine how motion is internally represented within the transformer layers. We hypothesize that while each DiT block contributes to both spatial and temporal reasoning, their relative importance varies. To efficiently control motion without injecting to the full model, we identify a subset of layers, denoted as Motion Layers, that are most critical for motion dynamics. Given an input image I , subject token s in the text condition, and a binary mask of the subject region M_f , we obtain the initial latent noise and track the attention maps $A_{\ell,s,f}^t$ between the subject token and spatial latent features throughout generation, where f is the frame number, t

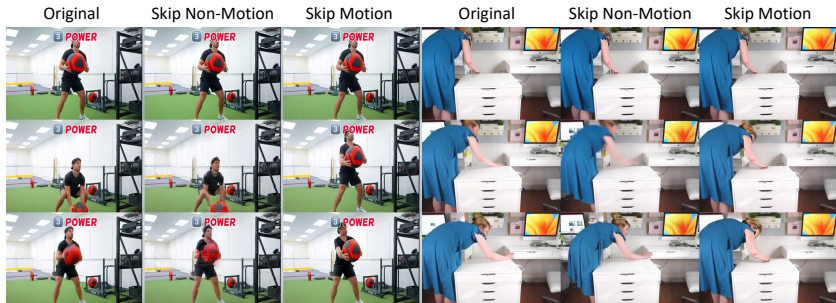


Fig. 5: Layer skipping. Skipping Non-Motion Layers mainly introduces artifacts, whereas skipping Motion Layers disrupts motion dynamics and temporal coherence.

is the timestep and ℓ denotes the layer number. Following the findings of [10], we consider both the text-to-video and video-to-text attention directions, and compute their average to capture bidirectional dependency between visual and textual modalities. We then compute similarity score, S_ℓ , between the binary mask M_f and the attention map for each layer. This is computed by averaging $A_{\ell,s,f}^t$ through all attention heads and applying frame-wise normalization. Finally, we sum the normalized values inside and outside the mask to calculate Attention Score as follows:

$$S_\ell = \frac{\sum_{f,t} M_f \otimes A_{\ell,s,f}^t}{\sum_{f,t} A_{\ell,s,f}^t}, \quad (2)$$

Intuitively, layers with higher S_ℓ exhibit stronger focus on the entirety of the moving subjects across all frames, strongly attending to their full motions (video-to-text attention) and also driving them (text-to-video attention), indicating their greater contribution towards the generated motions. We show the individual layer analysis in Fig. 3 and mark the Motion Layers as red. We also visualize the attention maps of Motion Layers and selected Non-Motion Layers in Fig. 4. As shown in Fig. 3, we observe a clear separation in attention score after the 11th layer, and we therefore set the top-11 layers as Motion Layers. See the supplementary material for the box plot with error bars.

To experimentally validate that the identified Motion Layers are responsible for motion formation, we conduct a controlled layer-skipping experiment using online videos of InterPose [60] dataset. We first generate 60 videos using our full model. For each video, we then sample two sets of three layers: three randomly selected layers from Motion Layers, and three randomly selected layers from 11 lowest scoring layers among Non-Motion Layers. Using the same initial random noise, we generate two additional outputs by skipping the selected layers in each set, resulting in a triplet per sample: the original generated video, the Motion Layers skipped video, and the Non-Motion Layers skipped video. This design allows us to isolate the effect of removing motion-relevant layers and removing layers that are less relevant according to the Attention Score.

Method	$\mathcal{J}\uparrow$	$\mathcal{F}\uparrow$	$\mathcal{J}\&\mathcal{F}\uparrow$	HOTA \uparrow
Skip Motion Layers	60.1	59.9	60.0	57.3
Skip Non-Motion Layers	77.7	81.1	79.4	82.3

Table 1: Layer analysis for motion formation. We generate videos skipping the randomly selected 3 Motion Layers and Non-Motion Layers, and report the tracking metrics.

Video Type	VQA Score
Generated Video	0.4540
Skip Motion Layers	0.2742
Skip Non-Motion Layers	0.4068

Table 2: Layer analysis on text-to-video metric. We generate video triplets, using the base model, skipping the selected 3 Motion Layers, Non-Motion Layers, and report text-to-video alignment.

For evaluation, we extract the subject mask from the generated videos using Grounding DINO [33] and Segment Anything 2 [44], and consider the original video masks as pseudo-ground truth tracking labels. We then evaluate the generated videos with tracking metrics that measure *motion consistency*, reporting \mathcal{J} , \mathcal{F} [41], and HOTA [35, 36] scores. See the supplementary material for more details about the metrics. As shown in Table 1, skipping Non-Motion Layers results in significantly higher tracking scores than skipping Motion Layers, indicating that removing Non-Motion Layers has less effect on motion formulation, whereas removing Motion Layers disrupts the structure of the subject motion.

In addition to motion consistency, we evaluate *semantic alignment* between the input text description and the generated videos using the VQA score [5, 31]. Table 2 shows that the original generations achieve the highest alignment, and that skipping Non-Motion Layers produces only a small difference as compared to the original results. In contrast, skipping Motion Layers leads to a significant drop in VQA score, suggesting that these layers are also important for text-to-motion alignment.

Finally, in Fig. 5 we observe that, while skipping Non-Motion Layers introduces visual degradation, such as noise or local patch artifacts, the overall motion remains mostly consistent with the original generation. In contrast, skipping Motion Layers changes the motion pattern drastically and can lead to critically degraded outputs, including incorrect dynamics or unrealistic results. Together, these results provide direct evidence that the proposed Motion Layers identification captures layers that are critical for video motion formation.

Motivated by this analysis, we apply the mask-condition injection to Motion Layers, focusing learning capacity on motion-related blocks while preserving the spatial appearance priors of the base model.

4.2 Mask Adapter

The Mask Adapter $\mathcal{MA}(\cdot)$ learns to project binary spatiotemporal masks into latent-space delta features that condition the video generation process. Given a binary mask tensor $M \in \{0, 1\}^{B \times 1 \times T \times H \times W}$, we first map it to the latent dimension $Z_t \in \mathbb{R}^{B \times C \times \frac{T}{4} \times \frac{H}{8} \times \frac{W}{8}}$. We spatially downsample the mask and temporally compress it by applying a logical OR operation across every non-overlapping

window of four consecutive frames. Then we input the downscaled and mean-normalized mask through the Mask Adapter $\mathcal{MA}(\cdot)$, which predicts the latent-space residual $\Delta Z = \mathcal{MA}(M)$ that modulates the dynamics of the video generation process. We visualize the mask projections in Fig. 2, demonstrating that it learns to affect the subject’s occupied region, and successfully adapts the surrounding interactions.

LoRA on Motion Layers: To adapt motion behavior while minimizing overfitting, we apply LoRA into each attention projection across Motion Layers. Only LoRA and the MaskAdapter parameters are updated during training, while the base model remains frozen.

4.3 Cosine-weighted Latent Injection

While implementing LoRA on motion layers is already effective, we observe that the model is also sensitive to when the condition is injected in the denoising process. Intuitively, we hypothesize that earlier denoising steps (close to Gaussian noise) are more crucial for mask-motion alignment, as they determine the large motions (i.e., rough movements shapes and silhouettes) that the subsequent denoising steps refine. Let the step index $s \in \{0, \dots, \tau - 1\}$ and normalized timestep $t_s = \frac{s}{\tau - 1}$. The cosine scheduler weight is defined as

$$w_s = \frac{1}{2}(1 + \cos(\pi t_s)), \quad (3)$$

so that $w_0 = 1$ and $w_{\tau-1} = 0$. At step s , the latent update is

$$\tilde{Z}_t^{(s)} = Z_t^{(s)} + w_s \cdot \Delta Z. \quad (4)$$

This schedule ensures that mask-conditioned motion guidance is strong in early steps and smoothly fades as the velocity prediction converges.

5 Experiments

We evaluate CoMoGen under mask guidance and ask whether a single binary mask sequence of a moving subject is sufficient to induce realistic interactions with the surrounding scene. Our evaluation covers two complementary settings that probe controllability, interaction quality, and overall video realism. In Section 5.2, we analyze **object interactions** in a synthetic environment using CLEVRER [57]. In Section 5.3, we study **human-object interactions** and measure how well the model reproduces subject motion and physical contact between humans and manipulated objects. We compare our method with state-of-the-art controllable methods: InterDyn [1], Go-with-the-flow (GoFlow) [9], and MagicMotion [30]. We report results of InterDyn*, where we reproduce their method for both datasets.

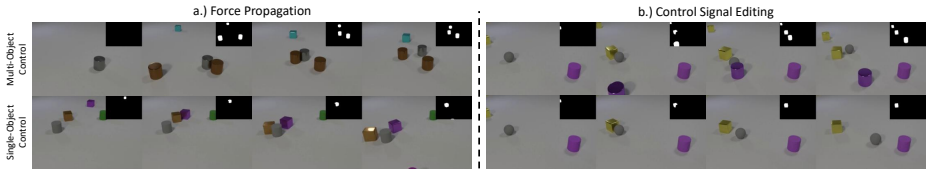


Fig. 6: Results on human-object interaction. We present generation results for (a) Force Propagation and (b) Control Signal Editing. For (b), we use the same input image with different control signals.

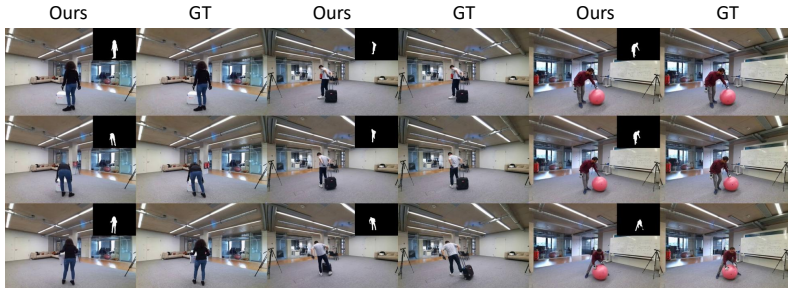


Fig. 7: Results on human-object interaction. We present generation results and the corresponding ground truths for different objects (box, luggage bag, and ball).

5.1 Dataset

We use two different datasets CLEVRER [57] and BEHAVE [6], and train two different models on each dataset. CLEVRER [57] provides synthetic videos with multiple objects undergoing collision events. CLEVRER provides 10k training and 5k validation videos. We use all videos in the training dataset and use a subset of 50 videos of the validation dataset. We use object-centric CLEVRER dataset to test the force propagation, counterfactual dynamics and motion fidelity similar to InterDyn [1]. BEHAVE [6] contains human-object interactions captured in real scenes, including strong occlusions, non-rigid human motion, and contact rich manipulation. We use 4k video subset of the dataset for training and 50 video subset for validation. In our setting, we provide only the human mask as a control and interaction signal, and we evaluate whether the generated videos preserve temporally coherent human motion while producing plausible responses.

5.2 Object Collisions and Reaction Dynamics

We show that CoMoGen can successfully alter the motion of the controlled object by providing a mask. We observe force propagation not only between the controlled and uncontrolled objects, but also among the uncontrolled objects themselves. In Fig. 6 (Force Propagation), we show this propagation. In the single-object example (bottom), by controlling only the purple cube entering

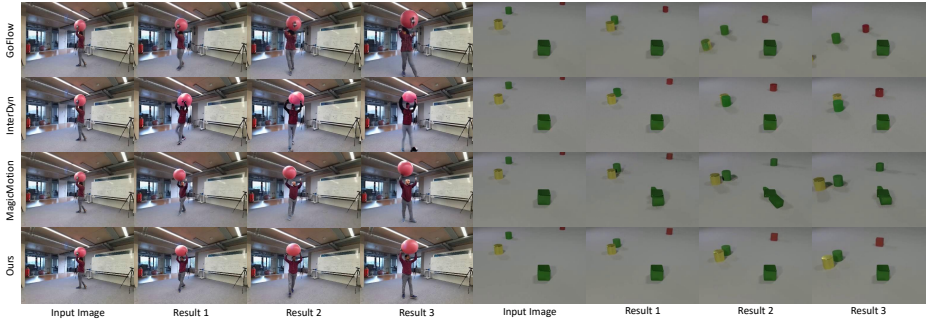


Fig. 8: Qualitative comparison on human-object interactions and object collision events. Our method successfully captures the human-object interactions and object collision events.

from the top, CoMoGen causes it to collide with and move the brown cube (controlled-uncontrolled interaction). Then, the brown cube collides with the gray cylinder and sets it into motion (uncontrolled-uncontrolled interaction).

We further show that modifying the control signal results in different outcomes, as shown in Fig. 6 (Control Signal Editing). In the first example (top), when two objects (the yellow cube and the purple cylinder) are controlled, the gray sphere first collides with the yellow cube and moves towards the purple cylinder, colliding with it. In the second example (bottom), we changed the control signal to only include the yellow cube, and the interactions of the gray sphere is also modified accordingly by our model.

In Table 3 (CLEVRER), we compare our method with Go-with-the-Flow (GoFlow) [9], InterDyn* [1], and MagicMotion [30]. Overall, the results show that the proposed intervention improves video-level realism while maintaining strong similarity to the ground truth. We consistently observe improvements in temporal realism (lower FVD), which aligns with our goal of generating temporally coherent dynamics.

Qualitative comparisons in Fig. 8 further support this conclusion. Baseline methods may produce plausible motion but often blur the causal structure of the event. In contrast, our method better preserves collision-driven changes and remain temporally stable after the interaction. Refer to our video in supplemental material to observe the videos qualitatively.

5.3 Human-Object Interaction with Human Mask Conditioning

Besides altering the motion of rigid synthetic objects, CoMoGen can also guide non-rigid subjects with complex motion: humans. Although we provide only the mask of the moving subject, CoMoGen can generate the resulting human-object interactions, including grasping, object displacement aligned with hand or foot motion, and object position changes consistent with body rotation.

Method	CLEVRER				BEHAVE			
	SSIM \uparrow	PSNR \uparrow	LPIPS \downarrow	FVD \downarrow	SSIM \uparrow	PSNR \uparrow	LPIPS \downarrow	FVD \downarrow
GoFlow [9]	0.9117	26.56	0.1085	341.01	0.5044	19.21	0.1823	617.24
InterDyn* [1]	0.8275	25.16	0.1632	358.02	0.5006	16.98	0.1893	720.14
MagicMotion [30]	0.7612	23.16	0.3315	466.51	0.7718	23.28	0.1191	694.41
Ours	0.9252	27.12	0.1732	258.52	0.7940	22.99	0.0721	327.63

Table 3: Quantitative comparison. We compare our method with state-of-the-art controllable video generation models.

Method	Inference Training		Setting	SSIM \uparrow PSNR \uparrow LPIPS \downarrow FVD \downarrow			
InterDyn [1]	100	100	LoRA on Non-Motion Layers	0.7787	21.81	0.0922	371.96
MagicMotion [30]	100	100	w/o Cosine-weighted injection	0.7938	22.99	0.0821	336.63
Ours	1.84	3.17	Ours	0.7940	22.99	0.0721	327.63

Table 4: Efficiency comparison. We report the percentage of additional parameters. **Table 5: Quantitative Ablation Study.** We evaluate selective layer injection and cosine-weighted injection in the human-object interaction setting.

In Fig. 7, we show interactions with three different objects. CoMoGen produces plausible human-object interactions by conditioning only on the subject mask, without requiring either object masks or explicit object motion guidance.

In Table 3 (BEHAVE), we compare our method with the baselines and observe consistent improvements in video fidelity, while maintaining strong performance across reconstruction metrics. Fig. 8 provides a qualitative comparison. The baselines often produce noticeable artifacts under complex motions, whereas our method generates more temporally consistent results. Refer to our video in supplemental material to observe the videos qualitatively.

5.4 Discussion on Out-of-distribution Robustness and Efficiency

We show that by applying text-guided edits to the input images, we can generate interactions for fictional or out-of-distribution characters, where Fig. 10 shows the out-of-distribution inputs remain compatible with our framework and the resulting videos preserve coherent motion. At the same time, we avoid the heavy conditioning used by recent mask-conditioned video generation baselines, which typically rely on a ControlNet-style branch that duplicates the backbone (e.g., a trainable copy of the frozen model), which adds 100% extra parameters at both inference and training (see Tab. 4). In contrast, our MaskAdapter is just two lightweight convolutional layers followed by a linear projection, adding only 1.84% parameters at inference, while training uses compact LoRA updates (an additional 1.33%), for a total of 3.17% extra parameters during training. Overall, CoMoGen maintains qualitative robustness under appearance shifts while being markedly more parameter-efficient than prior mask-conditioned approaches.

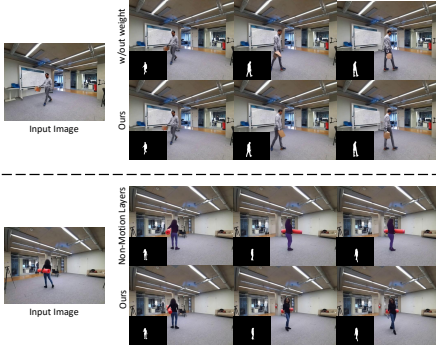


Fig. 9: Qualitative ablation. Top: removing cosine-weighted latent injection introduces textural artifacts. Bottom: training LoRA on random non-motion layers weakens motion control.

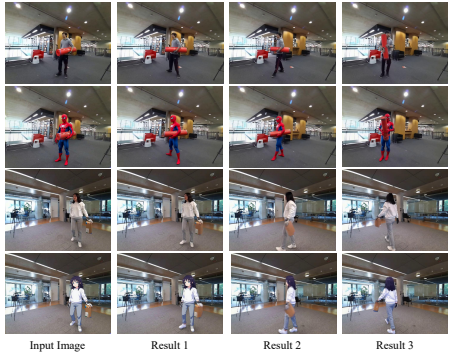


Fig. 10: Out-of-distribution edits. We edit input images with a text-guided editor [29] and show that generated interactions remain coherent on fictional characters.

5.5 Ablation Study

We ablate the effects of cosine-weighted latent injection, and restricting LoRA updates to Non-Motion Layers. Fig. 9 and Table 5 summarize the results. A key design choice is adapting only Motion Layers. To verify the layer selection, we swap Motion Layers with an equal number of randomly chosen Non-Motion Layers. As shown in Fig. 9 (bottom-left), training on random Non-Motion Layers loses precise controllability, consistent with the quantitative drop in Table 5. We also ablate the cosine-weighted latent schedule by applying the residual ΔZ with a constant weight across all steps. As shown in Fig. 9 (top row), this introduces undesirable textural artifacts and degrades all metrics (Table 5), suggesting that overly strong late-step conditioning disrupts refinement of fine details. The cosine schedule mitigates this by emphasizing mask alignment early while preserving refinement capabilities in later denoising steps.

6 Conclusion

We presented CoMoGen, a controllable video generation framework that produces realistic interactive dynamics from a single binary steering mask sequence conditioned on an input image. We show that motion formation in Multi Modal Diffusion Transformers is concentrated in Motion Layers, enabling targeted control. Our lightweight MaskAdapter injects mask derived latent residuals through Motion Layers with cosine scheduling and layer-restricted LoRA, resulting precise motion and coherent interactions with minimal overhead.

A remaining challenge arises under extreme and prolonged occlusion, where objects disappear entirely and later re-emerge, making identity recovery difficult for the video model. CoMoGen demonstrates that precise control does not

require complex inputs: temporally aligned mask guidance, applied at the right transformer layers, is enough to produce realistic scene dynamics. This formulation brings controllable video generation closer to applications where mask guidance can drive complex motion and interactions.

References

1. Akkerman, R., Feng, H., Black, M.J., Tzionas, D., Abrevaya, V.F.: Interdyn: Controllable interactive dynamics with video diffusion models. In: Proceedings of the Computer Vision and Pattern Recognition Conference. pp. 12467–12479 (2025)
2. Alhaija, H.A., Alvarez, J., Bala, M., Cai, T., Cao, T., Cha, L., Chen, J., Chen, M., Ferroni, F., Fidler, S., et al.: Cosmos-transfer1: Conditional world generation with adaptive multimodal control. arXiv preprint arXiv:2503.14492 (2025)
3. Avrahami, O., Patashnik, O., Fried, O., Nemchinov, E., Aberman, K., Lischinski, D., Cohen-Or, D.: Stable flow: Vital layers for training-free image editing. In: Proceedings of the Computer Vision and Pattern Recognition Conference (CVPR). pp. 7877–7888 (June 2025)
4. Bahmani, S., Skorokhodov, I., Qian, G., Siarohin, A., Menapace, W., Tagliasacchi, A., Lindell, D.B., Tulyakov, S.: Ac3d: Analyzing and improving 3d camera control in video diffusion transformers. Proc. CVPR (2025)
5. Bai, S., Chen, K., Liu, X., Wang, J., Ge, W., Song, S., Dang, K., Wang, P., Wang, S., Tang, J., Zhong, H., Zhu, Y., Yang, M., Li, Z., Wan, J., Wang, P., Ding, W., Fu, Z., Xu, Y., Ye, J., Zhang, X., Xie, T., Cheng, Z., Zhang, H., Yang, Z., Xu, H., Lin, J.: Qwen2.5-vl technical report. arXiv preprint arXiv:2502.13923 (2025)
6. Bhatnagar, B.L., Xie, X., Petrov, I., Sminchisescu, C., Theobalt, C., Pons-Moll, G.: Behave: Dataset and method for tracking human object interactions. In: IEEE Conference on Computer Vision and Pattern Recognition (CVPR). IEEE (jun 2022)
7. Blattmann, A., Dockhorn, T., Kulal, S., Mendelevitch, D., Kilian, M., Lorenz, D., Levi, Y., English, Z., Voleti, V., Letts, A., Jampani, V., Rombach, R.: Stable video diffusion: Scaling latent video diffusion models to large datasets (2023), <https://arxiv.org/abs/2311.15127>
8. Blattmann, A., Rombach, R., Ling, H., Dockhorn, T., Kim, S.W., Fidler, S., Kreis, K.: Align your latents: High-resolution video synthesis with latent diffusion models. In: IEEE Conference on Computer Vision and Pattern Recognition (CVPR) (2023)
9. Burgert, R., Xu, Y., Xian, W., Pilarski, O., Clausen, P., He, M., Ma, L., Deng, Y., Li, L., Mousavi, M., Ryoo, M., Debevec, P., Yu, N.: Go-with-the-flow: Motion-controllable video diffusion models using real-time warped noise. In: CVPR (2025), licensed under Modified Apache 2.0 with special crediting requirement
10. Cai, M., Cun, X., Li, X., Liu, W., Zhang, Z., Zhang, Y., Shan, Y., Yue, X.: Ditctrl: Exploring attention control in multi-modal diffusion transformer for tuning-free multi-prompt longer video generation. arXiv:2412.18597 (2024)
11. Cao, M., Wang, X., Qi, Z., Shan, Y., Qie, X., Zheng, Y.: Masactrl: Tuning-free mutual self-attention control for consistent image synthesis and editing. In: Proceedings of the IEEE/CVF International Conference on Computer Vision (ICCV). pp. 22560–22570 (October 2023)
12. Chang, P., Tang, J., Gross, M., Azevedo, V.C.: How i warped your noise: a temporally-correlated noise prior for diffusion models. arXiv preprint arXiv:2504.03072 (2025)

13. Chefer, H., Alaluf, Y., Vinker, Y., Wolf, L., Cohen-Or, D.: Attend-and-excite: Attention-based semantic guidance for text-to-image diffusion models. *ACM Transactions on Graphics (TOG)* **42**, 1 – 10 (2023), <https://api.semanticscholar.org/CorpusID:256416326>
14. Esser, P., Kulal, S., Blattmann, A., Entezari, R., Müller, J., Saini, H., Levi, Y., Lorenz, D., Sauer, A., Boesel, F., Podell, D., Dockhorn, T., English, Z., Rombach, R.: Scaling rectified flow transformers for high-resolution image synthesis. In: *Proceedings of the 41st International Conference on Machine Learning. ICML'24*, JMLR.org (2024)
15. Geng, D., Herrmann, C., Hur, J., Cole, F., Zhang, S., Pfaff, T., Lopez-Guevara, T., Aytar, Y., Rubinstein, M., Sun, C., et al.: Motion prompting: Controlling video generation with motion trajectories. In: *Proceedings of the Computer Vision and Pattern Recognition Conference*. pp. 1–12 (2025)
16. Geng, D., Herrmann, C., Hur, J., Cole, F., Zhang, S., Pfaff, T., Lopez-Guevara, T., Doersch, C., Aytar, Y., Rubinstein, M., Sun, C., Wang, O., Owens, A., Sun, D.: Motion prompting: Controlling video generation with motion trajectories. *arXiv preprint arXiv:2412.02700* (2024)
17. Goel, S., Pavlakos, G., Rajasegaran, J., Kanazawa, A., Malik, J.: Humans in 4D: Reconstructing and tracking humans with transformers. In: *ICCV* (2023)
18. Google: A new era of intelligence with gemini 3. <https://blog.google/products-and-platforms/products/gemini/gemini-3/> (November 2025), accessed: 2026-01-21
19. Gu, Z., Yan, R., Lu, J., Li, P., Dou, Z., Si, C., Dong, Z., Liu, Q., Lin, C., Liu, Z., Wang, W., Liu, Y.: Diffusion as shader: 3d-aware video diffusion for versatile video generation control. *arXiv preprint arXiv:2501.03847* (2025)
20. Guo, Y., Yang, C., Rao, A., Liang, Z., Wang, Y., Qiao, Y., Agrawala, M., Lin, D., Dai, B.: Animatediff: Animate your personalized text-to-image diffusion models without specific tuning. *arXiv preprint arXiv:2307.04725* (2023)
21. Hertz, A., Mokady, R., Tenenbaum, J., Aberman, K., Pritch, Y., Cohen-Or, D.: Prompt-to-prompt image editing with cross-attention control. In: *The Eleventh International Conference on Learning Representations* (2023), https://openreview.net/forum?id=_CDixzkzeyb
22. Ho, J., Chan, W., Saharia, C., Whang, J., Gao, R., Gritsenko, A., Kingma, D.P., Poole, B., Norouzi, M., Fleet, D.J., et al.: Imagen video: High definition video generation with diffusion models. *arXiv preprint arXiv:2210.02303* (2022)
23. Ho, J., Jain, A., Abbeel, P.: Denoising diffusion probabilistic models. In: *Proceedings of the 34th International Conference on Neural Information Processing Systems. NIPS '20*, Curran Associates Inc., Red Hook, NY, USA (2020)
24. Ho, J., Salimans, T., Gritsenko, A., Chan, W., Norouzi, M., Fleet, D.J.: Video diffusion models. *Advances in neural information processing systems* **35**, 8633–8646 (2022)
25. Hu, E.J., yelong shen, Wallis, P., Allen-Zhu, Z., Li, Y., Wang, S., Wang, L., Chen, W.: LoRA: Low-rank adaptation of large language models. In: *International Conference on Learning Representations* (2022), <https://openreview.net/forum?id=nZvKeeFYf9>
26. Kim, T., Joo, H.: Target-aware video diffusion models. *arXiv preprint arXiv:2503.18950* (2025)
27. Kong, W., Tian, Q., Zhang, Z., Min, R., Dai, Z., Zhou, J., Xiong, J., Li, X., Wu, B., Zhang, J., et al.: Hunyuanvideo: A systematic framework for large video generative models. *arXiv preprint arXiv:2412.03603* (2024)

28. Kuang, Z., Cai, S., He, H., Xu, Y., Li, H., Guibas, L., Wetzstein, G.: Collaborative video diffusion: Consistent multi-video generation with camera control. In: The Thirty-eighth Annual Conference on Neural Information Processing Systems (2024), <https://openreview.net/forum?id=arHJ1YiY2J>
29. Labs, B.F., Batifol, S., Blattmann, A., Boesel, F., Consul, S., Diagne, C., Dockhorn, T., English, J., English, Z., Esser, P., Kulal, S., Lacey, K., Levi, Y., Li, C., Lorenz, D., Müller, J., Podell, D., Rombach, R., Saini, H., Sauer, A., Smith, L.: Flux.1 kontext: Flow matching for in-context image generation and editing in latent space (2025), <https://arxiv.org/abs/2506.15742>
30. Li, Q., Xing, Z., Wang, R., Zhang, H., Dai, Q., Wu, Z.: Magicmotion: Controllable video generation with dense-to-sparse trajectory guidance. In: Proceedings of the IEEE/CVF International Conference on Computer Vision (ICCV). pp. 12112–12123 (October 2025)
31. Lin, Z., Pathak, D., Li, B., Li, J., Xia, X., Neubig, G., Zhang, P., Ramanan, D.: Evaluating text-to-visual generation with image-to-text generation. arXiv preprint arXiv:2404.01291 (2024)
32. Ling, P., Bu, J., Zhang, P., Dong, X., Zang, Y., Wu, T., Chen, H., Wang, J., Jin, Y.: Motionclone: Training-free motion cloning for controllable video generation. In: The Thirteenth International Conference on Learning Representations (2025), <https://openreview.net/forum?id=aY3L65HgHJ>
33. Liu, S., Zeng, Z., Ren, T., Li, F., Zhang, H., Yang, J., Li, C., Yang, J., Su, H., Zhu, J., et al.: Grounding dino: Marrying dino with grounded pre-training for open-set object detection. arXiv preprint arXiv:2303.05499 (2023)
34. Loshchilov, I., Hutter, F.: Decoupled weight decay regularization. In: International Conference on Learning Representations (2019), <https://openreview.net/forum?id=Bkg6RiCqY7>
35. Luiten, J., Hoffhues, A.: Trackeval. <https://github.com/JonathonLuiten/TrackEval> (2020)
36. Luiten, J., Osep, A., Dendorfer, P., Torr, P., Geiger, A., Leal-Taixé, L., Leibe, B.: Hota: A higher order metric for evaluating multi-object tracking. *International Journal of Computer Vision* pp. 1–31 (2020)
37. Meral, T.H.S., Yesiltepe, H., Dunlop, C., Yanardag, P.: Motionflow: Attention-driven motion transfer in video diffusion models. arXiv preprint arXiv:2412.05275 (2024)
38. Montanaro, A., Aira, L.S., Aiello, E., Valsesia, D., Magli, E.: Motioncraft: Physics-based zero-shot video generation. In: The Thirty-eighth Annual Conference on Neural Information Processing Systems (2024), <https://openreview.net/forum?id=1vcWA24dxB>
39. Namekata, K., Bahmani, S., Wu, Z., Kant, Y., Gilitschenski, I., Lindell, D.B.: Sg-i2v: Self-guided trajectory control in image-to-video generation. In: The Thirteenth International Conference on Learning Representations (2025), <https://openreview.net/forum?id=uQjySppU9x>
40. Peebles, W., Xie, S.: Scalable diffusion models with transformers. In: 2023 IEEE/CVF International Conference on Computer Vision (ICCV). pp. 4172–4182 (2023). <https://doi.org/10.1109/ICCV51070.2023.00387>
41. Perazzi, F., Pont-Tuset, J., McWilliams, B., Van Gool, L., Gross, M., Sorkine-Hornung, A.: A benchmark dataset and evaluation methodology for video object segmentation. In: *Computer Vision and Pattern Recognition* (2016)
42. Qiu, H., Chen, Z., Wang, Z., He, Y., Xia, M., Liu, Z.: Freetraaj: Tuning-free trajectory control in video diffusion models. arXiv preprint arXiv:2406.16863 (2024)

43. Qiu, H., Chen, Z., Wang, Z., He, Y., Xia, M., Liu, Z.: Freetrajectory: Tuning-free trajectory control via noise guided video diffusion (2025), <https://openreview.net/forum?id=CU7QfWJ6nC>
44. Ravi, N., Gabeur, V., Hu, Y.T., Hu, R., Ryali, C., Ma, T., Khedr, H., Rädle, R., Rolland, C., Gustafson, L., Mintun, E., Pan, J., Alwala, K.V., Carion, N., Wu, C.Y., Girshick, R., Dollár, P., Feichtenhofer, C.: Sam 2: Segment anything in images and videos. arXiv preprint arXiv:2408.00714 (2024), <https://arxiv.org/abs/2408.00714>
45. Rombach, R., Blattmann, A., Lorenz, D., Esser, P., Ommer, B.: High-resolution image synthesis with latent diffusion models (2021)
46. Saharia, C., Chan, W., Saxena, S., Li, L., Whang, J., Denton, E., Ghasemipour, S.K.S., Gontijo-Lopes, R., Ayan, B.K., Salimans, T., Ho, J., Fleet, D.J., Norouzi, M.: Photorealistic text-to-image diffusion models with deep language understanding. In: Oh, A.H., Agarwal, A., Belgrave, D., Cho, K. (eds.) *Advances in Neural Information Processing Systems* (2022), <https://openreview.net/forum?id=08Ykn512A1>
47. Shi, X., Huang, Z., Wang, F.Y., Bian, W., Li, D., Zhang, Y., Zhang, M., Cheung, K.C., See, S., Qin, H., et al.: Motion-i2v: Consistent and controllable image-to-video generation with explicit motion modeling. *SIGGRAPH 2024* (2024)
48. Song, J., Meng, C., Ermon, S.: Denoising diffusion implicit models. In: *International Conference on Learning Representations* (2021), <https://openreview.net/forum?id=St1giarCHLP>
49. Sudhakar, S., Liu, R., Hoorick, B.V., Vondrick, C., Zemel, R.: Controlling the world by sleight of hand (2024), <https://arxiv.org/abs/2408.07147>
50. Tevet, G., Raab, S., Gordon, B., Shafir, Y., Cohen-or, D., Bermano, A.H.: Human motion diffusion model. In: *The Eleventh International Conference on Learning Representations* (2023), <https://openreview.net/forum?id=SJ1kSy02jwu>
51. Wan, T., Wang, A., Ai, B., Wen, B., Mao, C., Xie, C.W., Chen, D., Yu, F., Zhao, H., Yang, J., Zeng, J., Wang, J., Zhang, J., Zhou, J., Wang, J., Chen, J., Zhu, K., Zhao, K., Yan, K., Huang, L., Feng, M., Zhang, N., Li, P., Wu, P., Chu, R., Feng, R., Zhang, S., Sun, S., Fang, T., Wang, T., Gui, T., Weng, T., Shen, T., Lin, W., Wang, W., Wang, W., Zhou, W., Wang, W., Shen, W., Yu, W., Shi, X., Huang, X., Xu, X., Kou, Y., Lv, Y., Li, Y., Liu, Y., Wang, Y., Zhang, Y., Huang, Y., Li, Y., Wu, Y., Liu, Y., Pan, Y., Zheng, Y., Hong, Y., Shi, Y., Feng, Y., Jiang, Z., Han, Z., Wu, Z.F., Liu, Z.: Wan: Open and advanced large-scale video generative models. arXiv preprint arXiv:2503.20314 (2025)
52. Wang, X., Yuan, H., Zhang, S., Chen, D., Wang, J., Zhang, Y., Shen, Y., Zhao, D., Zhou, J.: Videocomposer: Compositional video synthesis with motion controllability. *Advances in Neural Information Processing Systems* **36**, 7594–7611 (2023)
53. Wang, Z., Yuan, Z., Wang, X., Li, Y., Chen, T., Xia, M., Luo, P., Shan, Y.: Motionctrl: A unified and flexible motion controller for video generation. In: *ACM SIGGRAPH 2024 Conference Papers*. pp. 1–11 (2024)
54. Wu, W., Li, Z., Gu, Y., Zhao, R., He, Y., Zhang, D.J., Shou, M.Z., Li, Y., Gao, T., Zhang, D.: Draganything: Motion control for anything using entity representation (2024), <https://arxiv.org/abs/2403.07420>
55. Yang, Z., Teng, J., Zheng, W., Ding, M., Huang, S., Xu, J., Yang, Y., Hong, W., Zhang, X., Feng, G., et al.: Cogvideox: Text-to-video diffusion models with an expert transformer. arXiv preprint arXiv:2408.06072 (2024)
56. Yatim, D., Fridman, R., Bar-Tal, O., Kasten, Y., Dekel, T.: Space-time diffusion features for zero-shot text-driven motion transfer. arXiv preprint arxiv:2311.17009 (2023)

57. Yi, K., Gan, C., Li, Y., Kohli, P., Wu, J., Torralba, A., Tenenbaum, J.B.: CLEVRER: collision events for video representation and reasoning. In: ICLR (2020)
58. Yin, S., Wu, C., Liang, J., Shi, J., Li, H., Ming, G., Duan, N.: Dragnuwa: Fine-grained control in video generation by integrating text, image, and trajectory. arXiv preprint arXiv:2308.08089 (2023)
59. Zhang, L., Rao, A., Agrawala, M.: Adding conditional control to text-to-image diffusion models (2023)
60. Zhang, Y., Butt, A.A., Varol, G., Laptev, I.: Interpose: Learning to generate human-object interactions from large-scale web videos. arXiv (2025)
61. Zhang, Z., Liao, J., Li, M., Dai, Z., Qiu, B., Zhu, S., Qin, L., Wang, W.: Tora: Trajectory-oriented diffusion transformer for video generation. In: Proceedings of the Computer Vision and Pattern Recognition Conference. pp. 2063–2073 (2025)
62. Zhang, Z., Liao, J., Li, M., Dai, Z., Qiu, B., Zhu, S., Qin, L., Wang, W.: Tora: Trajectory-oriented diffusion transformer for video generation. In: Proceedings of the Computer Vision and Pattern Recognition Conference. pp. 2063–2073 (2025)
63. Zheng, Z., Peng, X., Yang, T., Shen, C., Li, S., Liu, H., Zhou, Y., Li, T., You, Y.: Open-sora: Democratizing efficient video production for all. arXiv preprint arXiv:2412.20404 (2024)

A Implementation Details

We train models on two different datasets: one on CLEVRER [57] and one on BEHAVE [6]. This mirrors the experimental goal of isolating object-centric collision dynamics and human-centric interaction dynamics. Both models follow the same method described in the main paper, the only difference is the dataset. We train all experiments at 360p resolution. We optimize with AdamW [34] and a learning rate of 5×10^{-5} . Training proceeds in two stages: the MaskAdapter is trained for 1 epoch with the backbone frozen, after which we enable LoRA on the Motion Layers and fine-tune LoRA and the MaskAdapter jointly for 2 additional epochs. We use a batch size of two and train on a single NVIDIA H100 GPU.

B Base Model Details

CoMoGen builds upon HunyuanVideo-I2V [27], a rectified-flow based I2V generation framework that uses an MMDiT architecture [14]. Given an input image $I \in \mathbb{R}^{H \times W \times 3}$ and a text prompt, the image is first encoded into a latent representation using a pretrained 3DVAE encoder. The generation process operates in the spatiotemporal latent space, initializing a noised video latent $Z_t \in \mathbb{R}^{C \times \frac{T}{4} \times \frac{H}{8} \times \frac{W}{8}}$ where the temporal length follows the backbone constraint $T = 4n + 1$ (up to 129 frames). In the I2V setting, Z_{img} is injected into the first frame of the latent sequence to preserve identity and scene layout, and is also provided as an additional conditioning signal throughout generation, complementing the text condition.

We select HunyuanVideo-I2V as our base model, because the MMDiT design results in rich attention maps across layers and modalities, providing a natural handle for diagnosing where subject-centric motion is formed and where controllability can be injected. This motivates our method design, where we keep the base model mostly frozen and focus adaptation and conditioning on a small subset of Motion Layers identified by our layer analysis.

C Layer Analysis Details

We conduct layer analysis using 50 samples from the BEHAVE [6] dataset. We give simple prompts like "A man grabbing a backpack from the ground" or "A woman carrying a table", and calculate the mean of Text-to-Video and Video-to-Text attention with respect to the subject token (i.e man, woman). The detailed attention scores with error bars are reported in Fig. 11. It shows that attention scores are consistent across different samples where Motion Layers consistently results in higher Attention Scores.

For the layer-skipping evaluations based on the selected Motion Layers, we evaluate using 60 samples from the in-the-wild InterPose [60] dataset. We calculate \mathcal{J} , \mathcal{F} [41], and HOTA [35, 36] scores. Specifically, \mathcal{J} is the Jaccard index

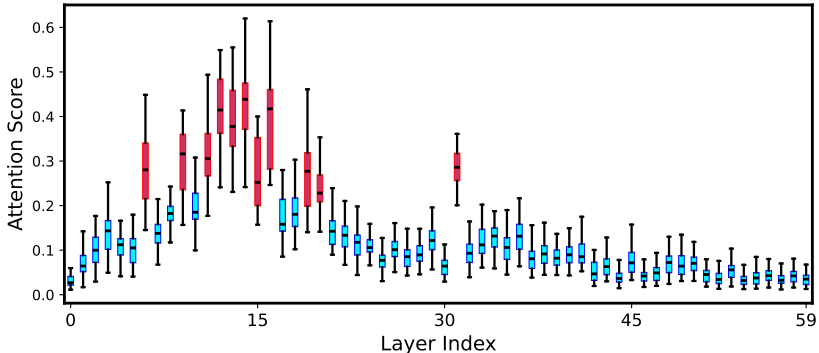


Fig. 11: Attention Score visualization across the layers with error bars.

(IoU) between the pseudo ground-truth mask and predicted mask which represents region similarity. \mathcal{F} is the contour accuracy, computed from contour precision/recall, emphasizing shape alignment. HOTA (Higher Order Tracking Accuracy) is a standard multi object tracking (MOT) metric that aids in measuring identity consistency, we report HOTA as an extra validation to our approach.

D Mask Robustness Evaluations

We also evaluate how robust our model is to variations in mask inputs.

Mask Frame Skipping. To examine the sensitivity of CoMoGen to incomplete mask guidance, we perform a mask robustness study in which we progressively remove portions of the input mask sequence at inference time. Specifically, starting from the original binary mask sequence, we evaluate four settings: using all masks, and retaining only one mask every 4, or 8 frames. For the skipped frames, the corresponding masks are blacked out, so that the model receives no subject guidance at those timesteps. Because retaining only one mask every eight frames can leave the compressed latent space without any control signal, we propagate the subsequent mask to the preceding skipped frame. We conduct this evaluation on a subset of 10 samples from the evaluation set. *Please refer to the video results in the project webpage.* When every mask is provided, the generated motion follows the intended trajectory most accurately. As masks are skipped more aggressively, we observe mild drift and reduced spatial precision in some frames, but the overall dynamics remain coherent in most cases. Even in the most sparse setting, where only one mask is retained every 8 frames, the model continues to recover temporally plausible motion rather than collapsing completely. Overall, these results indicate that CoMoGen is reasonably robust to temporally sparse mask conditioning, while still benefiting from denser mask supervision when precise control is required.

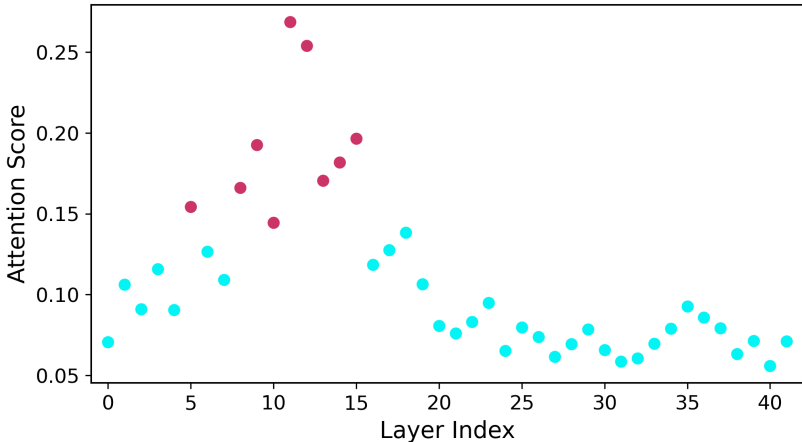


Fig. 12: Attention Score visualization of CogVideoX [55].

Method	$\mathcal{J} \uparrow$	$\mathcal{F} \uparrow$	$\mathcal{J}\&\mathcal{F} \uparrow$	HOTA \uparrow
Skip Motion Layers	39.4	32.0	35.7	36.5
Skip Non-Motion Layers	53.5	48.3	50.9	55.0

Table 6: Layer analysis for CogVideoX [55]. We generate videos skipping the randomly selected 3 Motion Layers and Non-Motion Layers, and report the tracking metrics for CogvideoX DiT model.

In the Wild Setting. To further evaluate generalization beyond the benchmark datasets, we consider an in-the-wild setting using online videos obtained from the InterPose dataset [60]. These videos exhibit larger appearance variation and less constrained scene structure than the training data (i.e., BEHAVE [6]), which tests whether the same mask-to-motion principle remains effective under more diverse real-world conditions. *Please refer to the qualitative results in the project webpage.*

E Layer Analysis for CogVideoX

In the paper, our layer analysis focused on HunyuanVideo [27], which is a recent DiT model. Here, we repeat the layer analysis for another DiT model CogVideoX-5B-I2V [55] following the same procedure as in the main paper. Specifically, we compute the Attention Score for each transformer block by measuring the alignment between the subject mask and the corresponding subject-token attention maps across inference steps, and then rank the layers accordingly. Based on this ranking, we define Motion Layers and Non-Motion Layers in CogVideoX (see Fig. 12), and perform the same controlled layer-skipping experiment used for the MMDiT backbone. For each generated sample, we keep the initial random noise

fixed and compare the original generation with two additional variants obtained by skipping randomly selected Motion Layers or randomly selected Non-Motion Layers. This allows us to isolate whether the layers identified by the attention-based ranking are in fact more critical to motion formation in CogVideoX as well. We measure tracking metrics and report the results in Tab. 6, which shows that skipping Motion Layers causes significantly more disruption to video quality.

F Applications

In this section, we highlight several potential applications of our model. *Please refer to the project webpage for qualitative examples of these applications.* All results are produced using the checkpoint trained on BEHAVE [6], demonstrating the model’s ability to generalize beyond its training setting.

F.1 Text-Guided Human Animation

In combination with existing open-source models, our approach can be used for text-guided human animation. Given a reference human image, we first estimate a human mesh using HMR2.0 [17]. We then employ the motion editing and inpainting capabilities of Motion Diffusion Model (MDM) [50] to generate a motion sequence from a text prompt. Finally, we render the animated mesh and extract the corresponding binary mask sequence, which is used as control input for our model.

F.2 Motion-to-Video Animation

Our method can also be used to convert generated motion into realistic videos. We first use MDM [50] to synthesize a motion sequence, then render the animated human mesh to obtain a binary mask sequence. Next, we transform the first frame with an image-to-image translation model, Gemini Nano Banana [18], and feed both the transformed first frame and the mask sequence into CoMoGen to generate the final realistic video.

F.3 Object Animation and Manipulation

Beyond human animation, our model can also be applied to object manipulation tasks. For instance, given an input image of an object, users can provide a sequence of handcrafted masks representing the desired motion or transformation. These masks may be handcrafted manually, or obtained simply through specifying the translation and rotation. Then, CoMoGen can be used to generate a video that follows the specified object movement.

F.4 Style Transfer

To demonstrate that CoMoGen can generalize to out-of-distribution subjects and visual domains, we first apply image-to-image translation to the input image [18, 29]. We then animate the translated image using CoMoGen, conditioned on the stylized first frame and its corresponding temporal binary mask sequence.